9242 *Biochemistry* **2009,** *48,* 9242–9249
DOI: 10.1021/bi900503k

BIOCHEMISTRY
including biophysical chemistry & molecular biology
Article

Conformation of the Phosphate D-Alanine Zwitterion in Bacterial Teichoic Acid from Nuclear Magnetic Resonance Spectroscopy†

Ravindranath Garimella, Jeffrey L. Halye, William Harrison, Phillip E. Klebba, and Charles V. Rice*

Department of Chemistry and Biochemistry, University of Oklahoma, 620 Parrington Oval, Room 208, Norman, Oklahoma 73019

Received March 24, 2009; Revised Manuscript Received July 7, 2009

ABSTRACT: The conformation of D-alanine (D-Ala) groups of bacterial teichoic acid is a central, yet untested, paradigm of microbiology. The D-Ala binds via the C-terminus, thereby allowing the amine to exist as a free cationic NH_3^+ group with the ability to form a contact ion pair with the nearby anionic phosphate group. This conformation hinders metal chelation by the phosphate because the zwitterion pair is charge neutral. To the contrary, the repulsion of cationic antimicrobial peptides (CAMPs) is attributed to the presence of the D-Ala cation; thus the ion pair does not form in this model. Solid-state nuclear magnetic resonance (NMR) spectroscopy has been used to measure the distance between amine and phosphate groups within cell wall fragments of *Bacillus subtilis*. The bacteria were grown on media containing ^{15}N D-Ala and β-chloroalanine racemase inhibitor. The rotational-echo double-resonance (REDOR) pulse sequence was used to measure the internuclear dipolar coupling, and the results demonstrate (1) the metal-free amine-to-phosphate distance is 4.4 Å and (2) the amine-to-phosphate distance increases to 5.4 Å in the presence of Mg^{2+} ions. As a result, the zwitterion exists in a nitrogen−oxygen ion pair configuration providing teichoic acid with a positive charge to repel CAMPs. Additionally, the amine of D-Ala does not prevent magnesium chelation in contradiction to the prevailing view of teichoic acids in metal binding. Thus, the NMR-based description of teichoic acid structure resolves the contradictory models, advances the basic understanding of cell wall biochemistry, and provides possible insight into the creation of new antibiotic therapies.

The cell wall of Gram-positive bacteria is composed of teichoic acids (lipoteichoic and wall teichoic acid, TAs) embedded in a peptidoglycan matrix (PG, Figure 1) (*1*−*3*). These biomolecules protect the bacterium from attack, transport nutrients, participate in cell-to-cell signaling, assist cell division, and aid in the attachment of bacteria to a substrate (*2*−*11*). Due to its role in bacterial infection and adhesion (*7*, *10*, *12*−*17*), teichoic acid has arisen as a potential target for antibiotic therapies (*15*−*24*). Assembly and transport events have been linked to several genes and their associated proteins. For *Bacillus subtilis* (*B. subtilis*), the teichoic acid backbone is composed of poly(glycerol phosphate), and the genes are denoted *tagABCEFGHO* (*25*−*27*). Poly(ribitol phosphate) forms the backbone of teichoic acid in *B. subtilis* W23 (*25*, *26*). Here, the necessary proteins are produced by genes *tarABIJKLDF*. Efforts are under way to identify the structure of the protein products and thereby aid the development of inhibitors to the teichoic acid synthetic pathway (*13*, *14*).

Teichoic acids have the same general structure (Figure 2); however, differences are seen in the anchoring groups and backbone composition (*1*, *3*, *32*). One form of TA is found anchored to the cell wall peptidoglycan (*33*, *34*). For *B. subtilis* wall teichoic acid (wall TA or WTA), D-alanine (D-Ala) and glucose groups are attached to the poly(glycerol phosphate) backbone (Figure 2). WTA from *Staphylococcus aureus* (*S. aureus*) has a poly(ribitol phosphate) backbone with *N*-acetylglucosamine (NAG) in place of glucose. In addition to WTA, TA can have lipid tails that anchor the polymer to the phospholipid bilayer. This lipoteichoic acid (LipoTA or LTA) has a poly(glycerol phosphate) with D-Ala, NAG, and hydroxyl groups decorating the backbone (*25*, *35*). The polyphosphate in both WTA and LTA is a long chain of 20−50 highly charged repeat units (*36*−*39*). While the NAG and hydroxyl side chains are charge neutral, an abundance of anionic character is created by phosphodiesters, only partially neutralized by the cationic D-Ala side chains. Charge neutralization is incomplete (*10*), giving teichoic acids a net negative charge and allowing them to form ionic bonds with surrounding fluids, dissolved ions, and the PG matrix. Gram-positive bacteria rely on the PG and TAs to chelate many types of metals from the extracellular milieu (*28*, *30*−*32*, *40*, *41*). The PG and TAs assist metal ion homeostasis across bacterial membranes by metal binding/uptake in the cell wall. TA is nearly 100% responsible for Ca^{2+} adsorption whereas it contributes 50% for K^+, Na^+, and Mg^{2+} binding (*42*). In addition, cadmium competitively displaces Ca^{2+} from the cell wall, likely due to the metal selectivity of teichoic acid (*43*). These binding observations can all be attributed to interactions with the diverse chemical functional groups of PG and TA.

These experiments offer a limited, macroscopic, view of metal binding. While the chemical functional groups have been identified, a complete explanation of the competitive binding trends requires structural data. A structural model has remained out of reach with the exception of one report by the Baddiley group. In the early 1970s, TAs were mixed with Mg^{2+} and analyzed with X-ray photoelectron spectroscopy, a technique which measures

†This work was supported in part by funds from the Oklahoma Center for the Advancement of Science and Technology (OCAST), the University of Oklahoma, National Institutes of Health Grant 6M53836 (P. E.K.), and National Science Foundation Grant MCB-0414694 (P.E. K.).

*To whom correspondence should be addressed. Telephone: (405) 325-0449. Fax: (405) 325-6111. E-mail: rice@ou.edu.

 Published on Web 09/11/2009

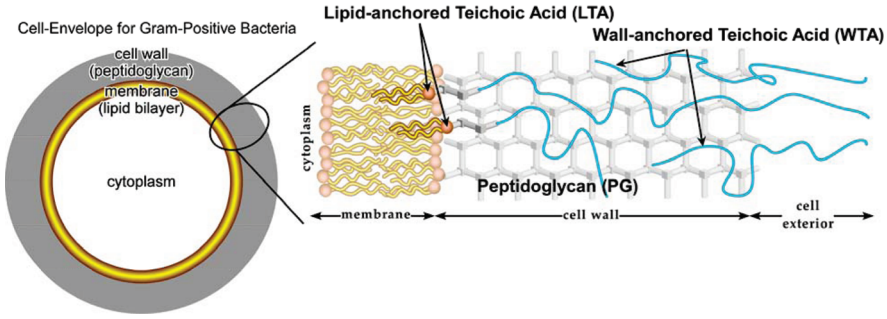

FIGURE 1: Teichoic acid, peptidoglycan, and membrane form the cell envelope of Gram-positive bacteria. Teichoic acids compose 50% of the cell wall mass. Not only are teichoic acids found within the peptidoglycan, they extend past the cell wall into the extracellular space. Teichoic acid exists in two configurations. In one, lipid tails anchor teichoic acid (LTA) to the membrane bilayer, and in the other configuration, teichoic acid attaches to the peptidoglycan, designated wall-anchored TA (WTA).

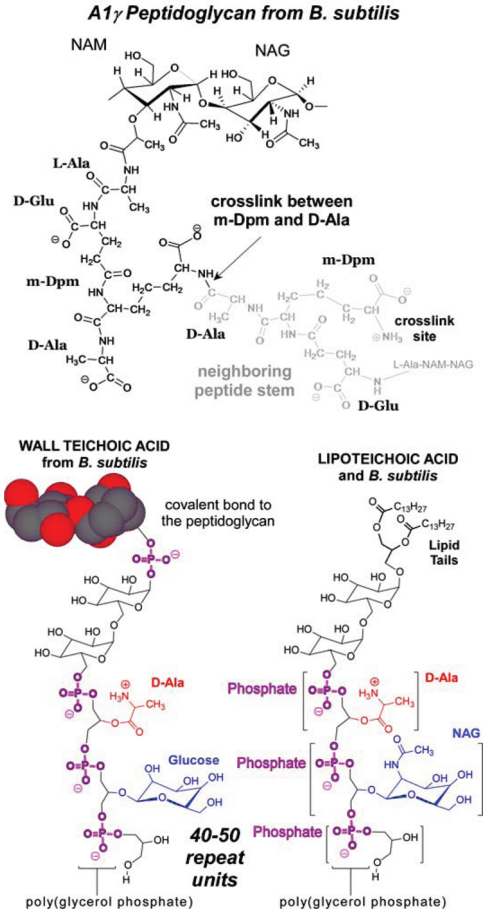

FIGURE 2: The many different constituents of TA facilitate chemical interactions with metal cations and the cell wall PG. Metals are attracted to the phosphates and carboxylates. The large number of phosphate groups permits timely NMR studies of the ^{31}P chemical environment. Carbon-13 and ^{15}N labels can be added to the D-Ala.

the energy of electrons ejected from the Mg^{2+} atom. Because the ejected electrons are also involved in chemical bonds, TA interactions alter the electronic energy, a perturbation detectable via XPS. Their results, reported in 1973 (*44*), were interpreted as monodentate Mg^{2+} binding by a single oxygen of the phosphate group. Additionally, the cationic α-NH_3 of D-Ala side chains of TA were suspected to inhibit metal binding by charge neutralization of the nearby phosphate. However, nuclear magnetic resonance (NMR) data from our group support a revised chelation model (*45*).

A different paradigm for teichoic acid structure is used to explain the repulsion of cationic antimicrobial peptides (CAMPs) by the bacterial cell wall. CAMPs bind to the anionic phospholipid bilayer and disrupt membrane integrity, resulting in bacterial death. The D-Ala groups of TA use the α-carboxyl for attachment to the phosphodiester backbone (Figure 2), an arrangement which leaves a positively charged α-amine group, which allows for a potential repulsive interaction with CAMPs. In wild-type strains, new CAMP-based antimicrobial therapies must overcome this D-Ala repulsion. Presently, we report rotational-echo double-resonance (REDOR) NMR data, whose interpretation creates a structural model in which the supposed salt bridge does not exist, a model which indicates separation by water molecules. More importantly, the presence of D-Ala does not prevent this site from chelating Mg^{2+}.

EXPERIMENTAL PROCEDURES

Sample Preparation. To produce cell walls with ^{15}N D-alanine labels, a 100 mL culture of *B. subtilis* was grown with defined media containing 10 mg of unenriched L-alanine and 10 mg of ^{15}N D-Ala (99%, Isotec) and harvested during the stationary phase. The alanine racemase inhibitor *β*-chloro-D-alanine (500 μg/mL) was added to prevent racemic conversion of the ^{15}N D-Ala.(*46*) Additional details of the growth media and the bacterial growth curve are included in the Supporting Information. Pepsin wall (WTA + peptidoglycan) samples were obtained from cells isolated from media using the following protocol (*47*−*49*). Cells were disrupted using a French press (14000 psi) and washed with doubly distilled water. The cell wall was then collected by centrifugation at 10000*g* for 20 min and treated with 2% Triton X-100 at 37 °C (30 min) and then 2% SDS (37 °C, 30 min) to remove the cytoplasmic membrane. The pellet was washed with ddH_2O and resuspended in 20 mM Tris-HCl, pH 7.8. Proteins and nucleic acids were removed with trypsin (200 μg/mL) and RNase/DNase (100 μg/mL) at 37 °C for 18 h. The pellet was washed with ddH_2O and resuspended in 20 mM sodium acetate, pH 4.0. The sample was subsequently treated with pepsin (100 μg/mL) for 2 h. Nucleic acid and protein removal was verified by spectroscopic analysis (260 and 280 nm). Prior to NMR analysis, the pellet was washed with ddH_2O and dried by lyophilization.

NMR Experiments. Solid-state NMR experiments were performed using a three-channel NMR spectrometer (^1H = 300 MHz, UnityInova; Varian, Inc.) and a 2 mm, three-channel, magic-angle-spinning (MAS) NMR probe (Doty probe with a revolution NMR spinning module). Drive and bearing gas were provided by dry, compressed air. The ^{15}N chemical shifts were referenced to external glycine. Data acquisition and processing

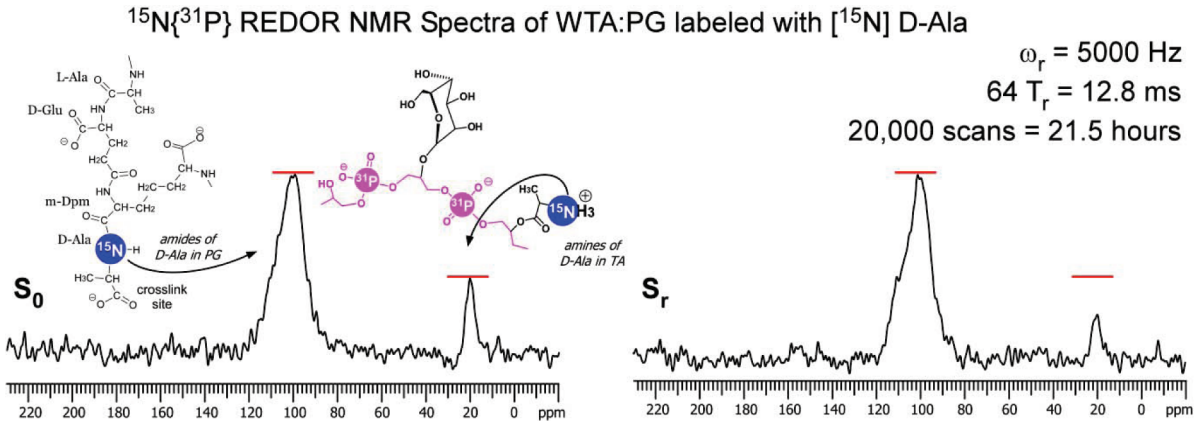

FIGURE 3: $^{15}N\{^{31}P\}$ REDOR spectra of WTA for a sample labeled with ^{15}N D-Ala. D-Ala is present as an amide in the A1γ PG and as an amine in the TA; hence two separate ^{15}N NMR signals are seen. The ^{31}P dephasing causes a reduction in the ^{15}N signal from enhanced T_2 relaxation, and the signal reduction can be used to measure the N−P internuclear distance. *B. subtilis* was grown in the presence of ^{15}N D-Ala, and the racemase inhibitor β-chloro-D-alanine prevents conversion into L-Ala. $B_0 = 7$ T, contact time = 2 ms, and spinning rate = 9 kHz. Chemical shift scale referenced to the ^{15}N amine signal of enriched glycine.

were accomplished with VNMRJ (version 1.1D) provided by Varian, Inc. REDOR data were collected using a sample spinning rate of 9000 Hz, cross-polarization (CP) contact time of 2000 μs, and ^1H decoupling at a power level of 50 kHz. The rf powers for the ^{15}N and ^{31}P channels were 50 kHz each. The XY-8 phase cycling scheme was used on both the ^{15}N and ^{31}P channels (*54*).

Distance determinations arise through the measurement of $^{15}N-^{31}P$ dipolar coupling. Although traditional CPMAS (cross-polarization under magic-angle spinning) averages away all dipolar interactions, one can turn to the solid-state NMR experiment, REDOR, to restore the dipolar interaction effects. Detailed mathematical and pictorial descriptions of REDOR have been reported (*54*−*57*). The dipole−dipole interaction causes transverse dephasing of the magnetization, reducing the signal intensity. Subtracting the "dephased echo" spectrum (S_r) from the full echo (S_0) spectrum provides a difference spectrum (ΔS), which is used to measure the dipolar coupling. The distance between ^{15}N and ^{31}P can be found by relating the intensity of ΔS to the dephasing time. However, as other T_2 processes may cause additional signal reduction, affecting both S_0 and S_r, a correction factor is applied by dividing ΔS by S_0, thereby giving the fraction of the total signal reduced exclusively by dipolar interaction. A plot of $\Delta S/S_0$ vs dephasing time yields the REDOR dephasing curve. The distance "r" is found by fitting the REDOR curve data to Bessel equations, which computationally provide an analytical solution to the nuclear spin Hamiltonians (*50*, *51*). This fitting is accomplished with the SIMPSON simulation software package (*52*), a method we have used previously to study metal binding of Li^+ ions in polymer electrolytes (*52*, *53*). The SIMPSON program (*58*) calculates a theoretical dephasing curve based on the nuclear spin system and the dipolar coupling constants. The distance between the interacting spins can be extracted from the strength of the dipole−dipole coupling using $D = (\mu_o h/4\pi)(\gamma^I\gamma^S/r^3)$, where D is the dipolar coupling constant, μ_o is the permittivity of free space, γ^I is the magnetogyric ratio of the dephasing nucleus (^{31}P), γ^S is the magnetogyric ratio of the observe nucleus (^{15}N), and r is the internuclear distance. Dipolar coupling constants were determined from multiple SIMPSON(*58*) simulations, each generating a theoretical REDOR dephasing curve. Using SIMPSON simulations to determine distance measurements and the accuracy of said measurements is well established. Although the error associated with these measurements cannot be measured quantitatively, the change in the dipolar coupling constant can be used to show a definitive change in the binding environment when metals are added to the cell wall samples. Additionally, a visual inspection of the theoretical REDOR curves shows that discrimination between measurements of ±0.1 Å is well within reason.

RESULTS

In Figure 3, the REDOR S_0 and S_r spectra are presented, showing two resolved signals for the labeled ^{15}N D-Ala amide and amine environments. In this sample, the amide signal is from the PG and the amine signal is from D-Ala of TA. The metal-free amine data points can be described by a theoretical REDOR curve with an ~4.4 Å N−P distance (Figure 4). The metal-free amide data (Figure 5) show that there is negligible heteronuclear dipolar coupling between the peptidoglycan amide sites and the neighboring teichoic acid phosphate groups. As our interest lies with the nearest neighboring heteronuclear dipolar coupling interactions, Figures 4 and 5 only show data within the range of the first 15 ms of dephasing time. SIMPSON simulations demonstrate that the first dephasing nucleus dominates this region.

The implication of these distance measurements is shown in Figure 6. First, the amine signal, arising solely from teichoic acid, can be used to determine if the amine actually forms a contact ion pair, the current paradigm for metal chelation by TAs. From energy-minimized structures (*45*), we know the amine−phosphate distance in the contact ion pair configuration is approximately 3.2 Å (model 1, Figure 6). Thus, the 4.4 Å amine−phosphate distance is inconsistent with the contact ion pair model. Therefore, a second model has been constructed to illustrate the 4.4 Å nitrogen−phosphorus distance. This new configuration provides space to allow for water molecules between the amine and phosphate groups (model 2, Figure 6).

These data refute the existence of the supposed contact ion pair. Nevertheless, the charges are close enough to each other to allow for partial charge neutralization which may affect metal binding. Therefore, $^{15}N\{^{31}P\}$ REDOR NMR experiments were performed to measure the N−P distance after the ^{15}N D-Ala labeled pepsin wall was mixed with $MgCl_2$. The metal-bound data show a longer internuclear distance of ~5.0 Å. The metal-bound amide data,

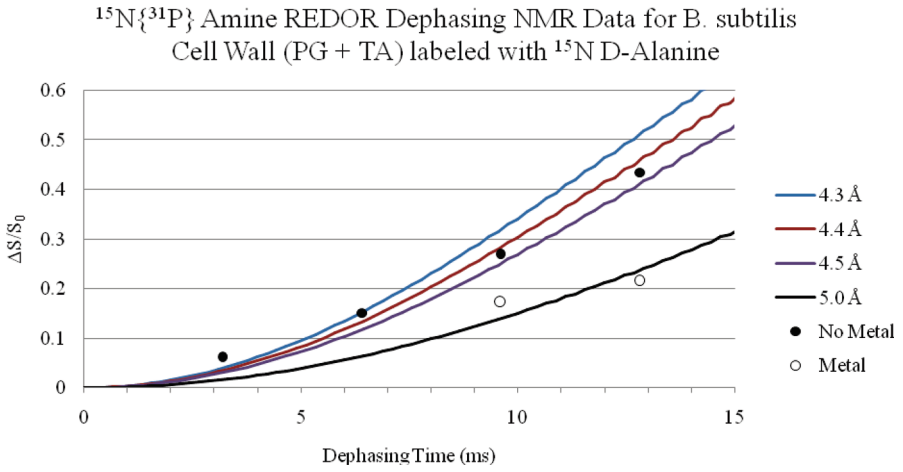

FIGURE 4: The amine signal intensities of spectra taken with different dephasing times are plotted with theoretical dephasing curves. The amine−P distance appears to be between roughly 4.4 Å in the unbound state while the metal-bound state shows 5.0 Å. Theoretical dephasing curves were generated from the SIMPSON program.

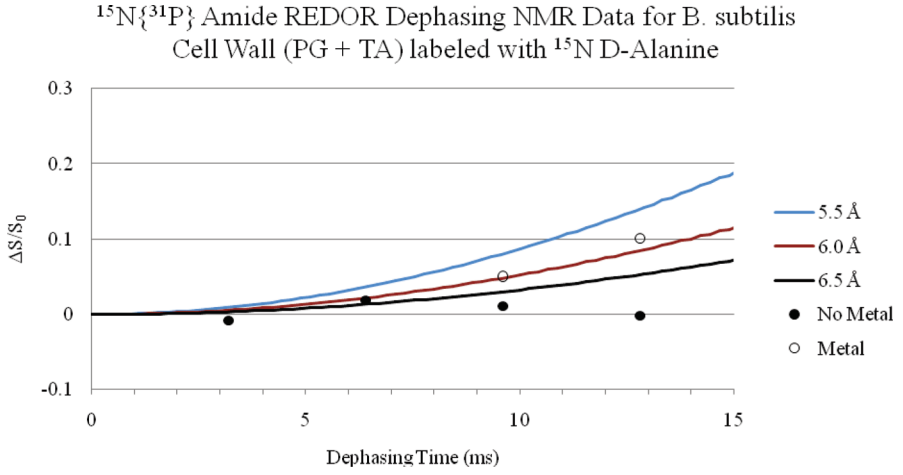

FIGURE 5: The amide signal intensities of spectra taken with different dephasing times are plotted with theoretical dephasing curves. With metals added, the amine−phosphate distance appears to decrease. This may be due to the creation of a multidentate binding pocket between teichoic acid and the peptidoglycan. However, additional data must be collected in order to correctly define this interaction.

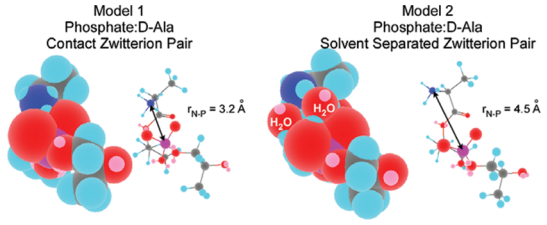

FIGURE 6: Energy-minimized structures of the phosphate−D-Ala fragment used to convert the internuclear distances into chemical models. The first model shows a contact ion pair with a distance of 3.2 Å, which does not replicate the 4.4 Å distance measured with REDOR. In the second model, a solvent-separated ion pair can be used to give the correct distance. Metal binding studies use the contact ion pair to explain trends whereas the separated ion pair is proposed to explain the repulsion of cationic antimicrobial peptides. Our data clearly support the latter model.

much like the unbound data, necessitate further experimentation in order to fully understand and confirm the decrease in N−P distance to ~6.0 Å. The metal-bound amine and amide data are also presented in Figures 4 and 5 and, when compared to the metal-free REDOR data, show that the metal cation pushes the amine farther away from the phosphate group, an orientation that should minimize (+) charge repulsions. We know from the 1-D ^{31}P CPMAS data that the phosphate CSA tensors are perturbed, a clear indication of metal binding (*45*). Combined with the present study, the solid-state NMR data contradict the current view of TA metal binding, in which the positively charged D-Ala neutralizes the phosphate anion and frustrates metal binding at this site. An energy-minimized model was created with an octahedral-coordinated hydrated bidentate Mg^{2+} cation with water molecules added to replicate charge shielding (Figure 7). The model shows a change in phosphate structure, with the two chelating oxygens now facing away from the amine, increasing the $NH_3^+-Mg^{2+}$ distance.

DISCUSSION

Ion pairs further can exist as three groups: salt bridge, nitrogen−oxygen (N−O) bridge, or a long-range ion pair (Figure 8) (*90*, *91*). The strongest interaction of these three would be the salt bridge, where the distance between at least one nitrogen−oxygen pair is within 4 Å. Likewise, the distance between the charged group central atoms (N−C in Figure 8 and N−P in teichoic acid) is also less than 4 Å. The nitrogen−oxygen bridge geometry is similar to the salt bridge, except that the central atoms of the charged groups no longer lie within 4 Å. In line with this trend, the long-range ion pair shows a geometry

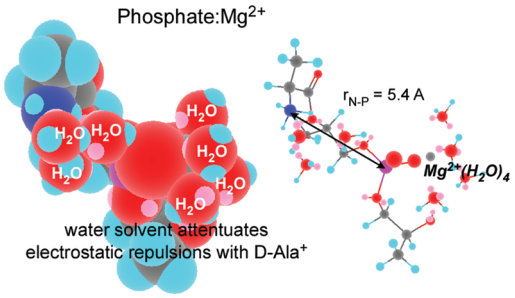

FIGURE 7: Energy-minimized structure of Mg^{2+} binding to the phosphate−D-Ala fragment. The model shows the solvent-separated ion pair with a distance of 5.4 Å. When compared to the structures in Figure 4, the phosphate ligand moves away from the amine of D-Ala. This new conformation maximizes electrostatic repulsion between the amine and metal and contradicts the accepted model that phosphates near D-Ala do not chelate metals because of charge neutralization in the TA backbone.

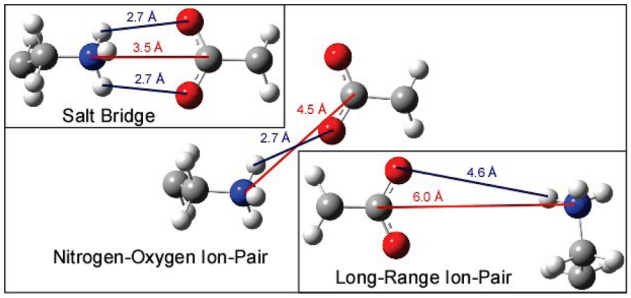

FIGURE 8: Ion pair models based on amino acid carboxylic acid and amine groups. Displays a visual representation of the distances involved in the three distinct classifications of ion pairing. Models created via Gaussview 4.0 and Canvas 8.

in which neither the charged group central atoms nor the nitrogen−oxygen pairs lie within the 4 Å distance. Additionally, a distance of less than 3.5 Å allows for the inference of a hydrogen-bonded salt bridge. These criteria outline a fairly specific molecular geometry, allowing for a particularly strong bonding interaction. This configuration results in protein−peptide stabilization or destabilization depending on the location and type of ion pairing interaction. Because these criteria deal with the interaction between two oppositely charged molecular species, they can be applied to the D-Ala−phosphate interactions of wall teichoic acid. With these criteria in mind, one can infer ion pairs of the nitrogen−oxygen bridging group based on our experimental NMR data. The $^{15}N\{^{31}P\}$ REDOR NMR data show that the cationic D-Ala and the anionic phosphate oxygen distance is ~4.4 Å.

Electrostatic forces play a fundamental and fairly predictable role in chemical interactions. In the case of D-Ala bound to teichoic acid, the labile nature of the charged cationic amine in close proximity to the anionic phosphate group(s) should result in the high probability of ion pairing. This configuration would neutralize the D-Ala cation. However, this model disagrees entirely with current experimental data which show that the presence of D-Ala in the cell wall of Gram-positive species provides resistance to CAMPs through a charge repulsion mechanism (*64*). This apparent contradiction can be explained by repeating REDOR-based distance measurements in the presence of Mg^{2+} because metals cations are required for bacterial survival and are found in relative abundance in nature. Thus, the analysis of REDOR NMR data collected on the bacterial cell wall in the presence of Mg^{2+} provides a more realistic insight into the structure and interactions of both peptidoglycan and teichoic acid.

Due to the phosphate pK_a of 2.1, TA metal coordination involves anionic PO_4^- ions at the majority of naturally occurring pH values. The fraction of PO_4^- anions is lowered by 80% at pH 1.5, which decreases Mg^{2+} binding by 75% (*28*). However, it is important to consider the pK_a of the amine of D-Ala, 9.69. At pH <9, the alanyl amino group exists as NH_3^+, perhaps forming an ion pair with the phosphate anion (Figure 2), possibly hindering the ability of the phosphate to participate in metal binding. In a seminal 1970 paper, Baddiley showed that chemical removal of D-alanine increased Mg^{2+} binding by 60% (*31*). Conversely, removal of the entire TA polymer from cell walls of *S. aureus* did not completely eliminate Mg^{2+} binding. This observation led to the conclusion that, in addition to TA, PG binds metal ions. Research over the next decade served to reveal the competitive binding nature of the cell wall. Addition of NaCl and KCl had little effect on Mg^{2+} concentration while $CaCl_2$ displaced Mg^{2+} in the cell wall (*28*).

Hoover and Gray studied a heat-sensitive strain of *S. aureus* showing that, without WTA, bacteria were susceptible to heat-induced death (*59*). Enhanced survivability from the presence of TA was linked to Mg^{2+} binding in the cell wall. As Ca^{2+} preferentially displaces magnesium, use of $CaCl_2$ also led to cell death. Later, Beveridge used electron microscopy and heavy metal staining to show metal binding to PG, presumably to the carboxyl groups (*60*). In 1980, Beveridge and Murray removed TA from *B. subtilis* cell walls to analyze the binding affinities for various alkali and alkali earth metal ions. Comparison with intact cell walls showed that Ca^{2+} binding requires TA, whereas Mg^{2+}, K^+, and Na^+ are bound by both TA and PG (*42*). Thus, the cell wall binding site was assigned to the carboxyl groups of the glutamic acid (Glu), diaminopimelate (Dap), and terminal D-Ala regions.

We show that a portion of the metal binding pocket involves phosphate anions near the D-Ala groups. Using electrostatics, it is possible to evaluate the forces between the zwitterion using $F = Q_1Q_2/4\pi\varepsilon_0\varepsilon r^2$, where Q_1 and Q_2 are the charges, ε_0 is the vacuum permittivity, ε is the dielectric constant, and r is the distance between charges. The salt bridge ion pair, without water separation, has a dielectric constant of 1 and, thus, should be favored over the nitrogen−oxygen ion pair, where the water has a dielectric constant of 78. Our data show a much different situation, explained by the entropy-driven formation of a solvent cage around the charges, which provides the negative Gibbs energy necessary for solvation. The divalent Mg^{2+} ion incurs preferential chelation by the phosphate, producing repulsion between the cation and the D-Ala, which results in the longer N−P distance. In the solvent-separated model, the ability to separate the charges with two water molecules results in greater shielding and a lower repulsive force. These structures provide a potential drug target; compounds that sequester metals are antimicrobial (*61*, *62*) given that the lack of metals causes cell wall destabilization, ultimately leading to membrane disruption and cell death.

A recent article by Karl Mueller's research group is an excellent example of how solid-state NMR spectroscopy can impact structural biology paradigms (*63*). Here, ^{31}P CPMAS spectra of mononucleotide deoxyadenosine monophosphate were collected to determine if it binds to the surface of aluminum oxide in a monodentate or a bidentate fashion. CSA tensors for

the phosphate demonstrated a bidentate binding, which was confirmed with computational chemistry calculations using Gaussian03. Subsequent $^{31}P\{^{27}Al\}$ REDOR studies confirmed that binding occurs at the octahedral aluminum oxide site rather than the tetrahedral site.

CAMP repulsion by teichoic acid due to cationic alanine groups is a structural model that was developed to explain genetic mutation studies (*64*). Mammalian production of CAMPs is an important means of protecting the host from microbial attack. The peptides contain 12−80 residues whose conformation is stabilized by cysteine−cysteine (Cys) disulfide bridges. The numerous arginine (Arg) and lysine (Lys) amino acids impart cationic properties that are only partially offset by anionic aspartate (Asp) and glutamate (Glu) residues. The basis for D-Ala addition to teichoic acid is attributed to the *dlt* operon. Mutants of *S. aureus* grown with the *dlt* operon disabled show a higher susceptibility to CAMPs. Without cationic alanyl repulsions from teichoic acid, hNP1-3 is a more effective antibiotic. The minimum inhibitory concentration (MIC) in the Δ*dlt* strain is 10 μg/mL, compared to over 100 μg/mL for the wild-type *S. aureus* (*65*). The *dlt* operon is also found in group A *Streptococci*. The MIC for cathelicidin was 3.5 μM in the Δ*dltA* mutant whereas the wild-type strain had a MIC of 14 μM.(*66*) Human cathelicidin is a 18 kDa peptide (*67*, *68*) with a net charge of +10 that acts by disrupting the membrane (*67*−*69*). The presence of D-Ala is required for *S. aureus* to protect against human group IIA phospholipase A_2, which is a 14 kDa polypeptide with a net charge of +12 to +17 (*70*). At 10 ng/mL, the viability of a *dltA*- *S. aureus* mutant dropped from 100% colony-forming units (CFU) to below 5% and to near zero when gIIA PLA_2 is added at 100 ng/mL. Conversely, removal of WTA entirely, with the *tagO* mutant, from *S. aureus* leads to enhanced resistance against gIIA PLA_2.(*71*) The mechanism of survival remains a mystery, although the authors suggest that the CAMP may be "bound electrostatically" to the PG. These binding sites could be shielded by the $-NH_3^+$ of WTA. Thus, the PLA_2 could move to the membrane when the PG binding sites are blocked.

Our heteronuclear dipolar coupling results from the teichoic acid amine site demonstrate that the alanine repulsion mechanism is viable because the amine does not form a salt bridge ion pair with the phosphate group. The probable nitrogen−oxygen ion pair configuration would allow for a long-range charge interaction at 4.4 Å but very little charge neutralization. Furthermore, the metal-bound configuration with an even larger internuclear distance and subsequent charge repulsion should have little to no charge neutralization at the amine site. Therefore, in either configuration, the D-Ala would be flexible, allowing for full charge repulsion of cationic antimicrobial peptides.

CONCLUSIONS

B. subtilis cell walls (teichoic acid and peptiodoglycan) were labeled with ^{15}N D-Ala and analyzed with solid-state NMR spectroscopy. Phosphorus−nitrogen distance measurements show that the zwitterion exists as a probable nitrogen−oxygen ion pair, contradicting the models used to explain metal binding trends. Subsequent measurements in the presence of Mg^{2+} ions reveal that metals bind in this area and the resultant charge repulsion pushes the D-Ala further away from the phosphate. These data support the model of teichoic acid structure used to explain repulsion of cationic antimicrobial peptides by the D-Ala group.

ACKNOWLEDGMENT

We thank Prof. Eric Brown (McMaster University) for helpful insight into teichoic acid biochemistry. Likewise, we thank Prof. Andreas Peschel (University of Tubingen) for helpful comments. We also thank Roger Frech (University of Oklahoma) for helpful discussions regarding solvent-separated ion pairs.

SUPPORTING INFORMATION AVAILABLE

The *B. subtilis* synthetic medium (BSSM) is described and the growth curve provided as a collection (PDF). This material is available free of charge via the Internet at http://pubs.acs.org.

REFERENCES

1. Graham, L. L., and Beveridge, T. J. (1994) Structural differentiation of the *Bacillus subtilis*-168 cell-wall. *J. Bacteriol. 176*, 1413–1421.
2. Neuhaus, F., and Baddiley, J. (2003) A continuum of anionic charge: Structures and functions of D-alanyl-teichoic acids in gram-positive bacteria. *Microbiol. Mol. Biol. 67*, 686.
3. Ginsburg, I. (2002) Role of lipoteichoic acid in infection and inflammation. *Lancet Infect. Dis. 2*, 171–179.
4. Courtney, H. S., Hasty, D. L., and Dale, J. B. (2002) Molecular mechanisms of adhesion, colonization, and invasion of group A streptococci. *Ann. Med. 34*, 77–87.
5. Tellefson, L. M., and Germaine, G. R. (1986) Adherence of *Streptococcus sanguis* to hydroxyapatite coated with lysozyme and lysozyme-supplemented saliva. *Infect. Immun. 51*, 750–759.
6. Tellefson, L. M., and Germaine, G. R. (1984) Effect of lysozyme on hydroxyapatite adherence of *S. sanguis*. *J. Dent. Res. 63*, 188–188.
7. Weidenmaier, C., Kristian, S. A., and Peschel, A. (2003) Bacterial resistance to antimicrobial host defenses—An emerging target for novel antiinfective strategies?. *Curr. Drug Targets 4*, 643–649.
8. Abachin, E., Poyart, C., Pellegrini, E., Milohanic, E., Fiedler, F., Berche, P., and Trieu-Cuot, P. (2002) Formation of D-alanyl-lipoteichoic acid is required for adhesion and virulence of *Listeria* monocytogenes. *Mol. Microbiol. 43*, 1–14.
9. Rose, R. (2000) The role of calcium in oral streptococcal aggregation and the implications for biofilm formation and retention. *Biochim. Biophys. Acta 1475*, 76–82.
10. Gross, M., Cramton, S. E., Gotz, F., and Peschel, A. (2001) Key role of teichoic acid net charge in *Staphylococcus aureus* colonization of artificial surfaces. *Infect. Immun. 69*, 3423–3426.
11. Fedtke, I., Gotz, F., and Peschel, A. (2004) Bacterial evasion of innate host defenses—The *Staphylococcus aureus* lesson. *Int. J. Med. Microbiol. 294*, 189–194.
12. Grundling, A., and Schneewind, O. (2007) Synthesis of glycerol phosphate lipoteichoic acid in *Staphylococcus aureus*. *Proc. Natl. Acad. Sci. U.S.A. 104*, 8478–8483.
13. Ginsberg, C., Zhang, Y. H., Yuan, Y. Q., and Walker, S. (2006) In vitro reconstitution of two essential steps in wall teichoic acid biosynthesis. *ACS Chem. Biol. 1*, 25–28.
14. Pohl, N. L. (2006) Building a bride to new antibiotics. *ACS Chem. Biol. 1*, 14–16.
15. Weidenmaier, C., Kokai-Kun, J. F., Kristian, S. A., Chanturiya, T., Kalbacher, H., Gross, M., Nicholson, G., Neumeister, B., Mond, J. J., and Peschel, A. (2004) Role of teichoic acids in *Staphylococcus aureus* nasal colonization, a major risk factor in nosocomial infections. *Nat. Med. 10*, 243–245.
16. Weidenmaier, C., Peschel, A., Kempf, V. A. J., Lucindo, N., Yeaman, M. R., and Bayer, A. S. (2005) DltABCD- and MprF-mediated cell envelope modifications of *Staphylococcus aureus* confer resistance to platelet microbicidal proteins and contribute to virulence in a rabbit endocarditis model. *Infect. Immun. 73*, 8033–8038.
17. Weidenmaier, C., Peschel, A., Xiong, Y. Q., Kristian, S. A., Dietz, K., Yeaman, M. R., and Bayer, A. S. (2005) Lack of wall teichoic acids in *Staphylococcus aureus* leads to reduced interactions with endothelial cells and to attenuated virulence in a rabbit model of endocarditis. *J. Infect. Dis. 191*, 1771–1777.
18. Pathania, R., and Brown, E. D. (2008) Small and lethal: Searching for new antibacterial compounds with novel modes of action. *Biochem. Cell Biol. 86*, 111–115.
19. Meredith, T. C., Swoboda, J. G., and Walker, S. (2008) Late-stage polyribitol phosphate wall teichoic acid biosynthesis in *Staphylococcus aureus*. *J. Bacteriol. 190*, 3046–3056.

20. Brown, S., Zhang, Y. H., and Walker, S. (2008) A revised pathway proposed for *Staphylococcus aureus* wall teichoic acid biosynthesis based on in vitro reconstitution of the intracellular steps. *Chem. Biol. 15*, 12–21.
21. Zhang, Y. H., Ginsberg, C., Yuan, Y. Q., and Walker, S. (2006) Acceptor substrate selectivity and kinetic mechanism of *Bacillus subtilis* TagA. *Biochemistry 45*, 10895–10904.
22. Scott, M. G., Gold, M. R., and Hancock, R. E. W. (1999) Interaction of cationic peptides with lipoteichoic acid and gram-positive bacteria. *Infect. Immun. 67*, 6445–6453.
23. Zorko, M., and Jerala, R. (2008) Alexidine and chlorhexidine bind to lipopolysaccharide and lipoteichoic acid and prevent cell activation by antibiotics. *J. Antimicrob. Chemother. 62*, 730–737.
24. Warshakoon, H. J., Burns, M. R., and David, S. A. (2009) Structure-activity relationships of antimicrobial and lipoteichoic acid-sequestering properties in polyamine sulfonamides. *Antimicrob. Agents 53*, 57–62.
25. Bhavsar, A. P., and Brown, E. D. (2006) Cell wall assembly in *Bacillus subtilis*: How spirals and spaces challenge paradigms. *Mol. Microbiol. 60*, 1077–1090.
26. Schertzer, J. W., Bhavsar, A. P., and Brown, E. D. (2005) Two conserved histidine residues are critical to the function of the TagF-like family of enzymes. *J. Biol. Chem. 280*, 36683–36690.
27. Bhavsar, A. P., Truant, R., and Brown, E. D. (2005) The TagB protein in *Bacillus subtilis* 168 is an intracellular peripheral membrane protein that can incorporate glycerol phosphate onto a membrane-bound acceptor in vitro. *J. Biol. Chem. 280*, 36691–36700.
28. Lambert, P. A., Hancock, I. C., and Baddiley, J. (1975) Interaction of magnesium-ions with teichoic-acid. *Biochem. J. 149*, 519–524.
29. Lambert, P. A., Hancock, I. C., and Baddiley, J. (1975) Influence of alanyl ester residues on binding of magnesium-ions to teichoic-acids. *Biochem. J. 151*, 671–676.
30. Heckels, J. E., Lambert, P. A., and Baddiley, J. (1977) Binding of magnesium-ions to cell-walls of *Bacillus subtilis*-W23 containing teichoic-acid or teichuronic acid. *Biochem. J. 162*, 359–365.
31. Heptinstall, S., Archibald, A. R., and Baddiley, J. (1970) Teichoic acids and membrane function in bacteria. *Nature 225*, 519.
32. Neuhaus, F., and Baddiley, J. (2003) A continuum of anionic charge: Structures and functions of D-alanyl-teichoic acids in gram-positive bacteria. *Microbiol. Mol. Biol. Rev. 67*, 686–723.
33. Archibald, A., Baddiley, J., Armstrong, J. J., and Hay, J. B. (1961) Teichoic acids and structure of bacterial walls. *Nature 191*, 570.
34. Baddiley, J. (1968) Teichoic acids and molecular structure of bacterial walls. *Proc. R. Soc. London, Ser. B 170*, 331.
35. Bhavsar, A. P., Erdman, L. K., Schertzer, J. W., and Brown, E. D. (2004) Teichoic acid is an essential polymer in *Bacillus subtilis* that is functionally distinct from teichuronic acid. *J. Bacteriol. 186*, 7865–7873.
36. Morath, S., Geyer, A., Spreitzer, I., Hermann, C., and Hartung, T. (2002) Structural decomposition and heterogeneity of commercial lipoteichoic acid preparations. *Infect. Immun. 70*, 938–944.
37. Heaton, M. P., and Neuhaus, F. C. (1994) Role of the D-alanyl carrier protein in the biosynthesis of D-alanyl-lipoteichoic acid. *J. Bacteriol. 176*, 681–690.
38. Volkman, B. F., Zhang, Q. Y., Debabov, D. V., Rivera, E., Kresheck, G. C., and Neuhaus, F. C. (2001) Biosynthesis of D-alanyl-lipoteichoic acid: The tertiary structure of apo-D-alanyl carrier protein. *Biochemistry 40*, 7964–7972.
39. Stadelmaier, A., Morath, S., Hartung, T., and Schmidt, R. R. (2003) Synthesis of the first fully active lipoteichoic acid. *Angew. Chem., Int. Ed. 42*, 916–920.
40. Beveridge, T. J., and Doyle, R. J. (1989) Metal ions and bacteria , Wiley, New York.
41. Beveridge, T. J., and Murray, R. G. E. (1976) Uptake and retention of metals by cell-walls of *Bacillus subtilis*. *J. Bacteriol. 127*, 1502–1518.
42. Beveridge, T. J., and Murray, R. G. E. (1980) Sites of metal-deposition in the cell-wall of *Bacillus subtilis*. *J. Bacteriol. 141*, 876–887.
43. Plette, A. C. C., Benedetti, M. F., and vanRiemsdik, W. H. (1996) Competitive binding of protons, calcium, cadmium, and zinc to isolated cell walls of a gram-positive soil bacterium. *Environ. Sci. Technol. 30*, 1902–1910.
44. Baddiley, J., Hancock, I. C., and Sherwood, P. M. (1973) X-Ray photoelectron studies of magnesium ions bound to cell-walls of gram-positive bacteria. *Nature 243*, 43–45.
45. Wickham, J., Halye, J., Kashtanov, S., Khandogin, J., and Rice, C. (2009) Revisiting magnesium chelation by teichoic acid with phosphorus solid-state NMR and theoretical calculations. *J. Phys. Chem. B 113*, 2177–2183.
46. Manning, J. M., Merrifie, Ne, Jones, W. M., and Gotschli, Ec. (1974) Inhibition of bacterial-growth by beta-chloro-D-alanine. *Proc. Natl. Acad. Sci. U.S.A. 71*, 417–421.
47. Amako, K., Umeda, A., and Murata, K. (1982) Arrangement of peptidoglycan in the cell-wall of *Staphylococcus* spp.. *J. Bacteriol. 150*, 844–850.
48. Umeda, A., Ueki, Y., and Amako, K. (1987) Structure of the *Staphylococcus aureus* cell-wall determined by freeze-substitution method. *J. Bacteriol. 169*, 2482–2487.
49. Umeda, A., Yokoyama, S., Arizono, T., and Amako, K. (1992) Location of peptidoglycan and teichoic-acid on the cell-wall surface of *Staphylococcus aureus* as determined by immunoelectron microscopy. *J. Electron Microsc. 41*, 46–52.
50. Mueller, K. T. (1995) Analytic solutions for the time evolution of dipolar-dephasing NMR signals. *J. Magn. Reson., Ser. A 113*, 81–93.
51. Mueller, K. T., Jarvie, T. P., Aurentz, D. J., and Roberts, B. W. (1995) The Redor transform—Direct calculation of internuclear couplings from dipolar-dephasing NMR data. *Chem. Phys. Lett. 242*, 535–542.
52. Wickham, J. R., York, S. S., Rocher, N. M., and Rice, C. V. (2006) Lithium environment in dilute poly(ethylene oxide)/lithium triflate polymer electrolyte from REDOR NMR spectroscopy. *J. Phys. Chem. B 110*, 4538–4541.
53. Wickham, J. R., Mason, R. N., and Rice, C. V. (2007) Solid-state NMR studies of the crystalline and amorphous domains within PEO and PEO: LiTf systems. *Solid State Magn. Reson. 31*, 184–192.
54. Gullion, T. (1998) Introduction to rotational-echo, double-resonance NMR. *Concepts Magn. Reson. 10*, 277–289.
55. McDowell, L. M., and Schaefer, J. (1996) High-Resolution NMR of biological solids. *Curr. Opin. Struct. Biol. 6*, 624–629.
56. Schaefer, J. (1996) Redor & Tedor, in Encyclopedia of Nuclear Magnetic Resonance (Harris, R. K., Ed.) pp 3983−3984, John Wiley, New York.
57. Gullion, T., and Schaefer, J. (1989) Rotational-echo double-resonance NMR. *J. Magn. Reson. 81*, 196–200.
58. Bak, M., Rasmussen, J. T., and Nielsen, N. C. (2000) SIMPSON. A general simulation program for solid-state NMR spectroscopy. *J. Magn. Reson. 147*, 296–330.
59. Hoover, D. G., and Gray, R. J. H. (1977) Function of cell-wall teichoic-acid in thermally injured *Staphylococcus aureus*. *J. Bacteriol. 131*, 477–485.
60. Beveridge, T. J., Forsberg, C. W., and Doyle, R. J. (1982) Major sites of metal-binding in *Bacillus licheniformis* walls. *J. Bacteriol. 150*, 1438–1448.
61. Maier, S. K., Scherer, S., and Loessner, M. J. (1999) Long-chain polyphosphate causes cell lysis and inhibits *Bacillus cereus* septum formation, which is dependent on divalent cations. *Appl. Environ. Microbiol. 65*, 3942–3949.
62. Kornberg, A. (1995) Inorganic polyphosphate—Toward making a forgotten polymer unforgettable. *J. Bacteriol. 177*, 491–496.
63. Fry, R. A., Kwon, K. D., Komarneni, S., Kubicki, J. D., and Mueller, K. T. (2006) Solid-state and computational chemistry study of monomucleotides adsorbed to alumina. *Langmuir 22*, 9281–9286.
64. Peschel, A. (2002) How do bacteria resist human antimicrobial peptides?. *Trends Microbiol. 10*, 179–186.
65. Peschel, A., Otto, M., Jack, R. W., Kalbacher, H., Jung, G., and Gotz, F. (1999) Inactivation of the dlt operon in *Staphylococcus aureus* confers sensitivity to defensins, protegrins, and other antimicrobial peptides. *J. Biol. Chem. 274*, 8405–8410.
66. Kristian, S. A., Datta, V., Weidenmaier, C., Kansal, R., Fedtke, I., Peschel, A., Gallo, R. L., and Nizet, V. (2005) D-Alanylation of teichoic acids promotes group A *Streptococcus* antimicrobial peptide resistance, neutrophil survival, and epithelial cell invasion. *J. Bacteriol. 187*, 6719–6725.
67. Nagaoka, I., Hirota, S., Yomogida, S., Ohwada, A., and Hirata, M. (2000) Synergistic actions of antibacterial neutrophil defensins and cathelicidins. *Inflammation Res. 49*, 73–79.
68. Gennaro, R., and Zanetti, M. (2000) Structural features and biological activities of the cathelicidin-derived antimicrobial peptides. *Biopolymers 55*, 31–49.
69. Shai, Y. (2002) Mode of action of membrane active antimicrobial peptides. *Biopolymers 66*, 236–248.
70. Koprivnjak, T., Peschel, A., Gelb, M. H., Liang, N. S., and Weiss, J. P. (2002) Role of charge properties of bacterial envelope in bactericidal action of human group IIA phospholipase A(2) against *Staphylococcus aureus*. *J. Biol. Chem. 277*, 47636–47644.
71. Koprivnjak, T., Weidenmaier, C., Peschel, A., and Weiss, J. P. (2008) Wall teichoic acid deficiency in *Staphylococcus aureus* confers selective resistance to mammalian group IIA phospholipase A(2) and human p-defensin 3. *Infect. Immun. 76*, 2169–2176.

72. Schleife, K., and Kandler, O. (1972) Peptidoglycan types of bacterial cell-walls and their taxonomic implications. *Bacteriol. Rev. 36*, 407–477.
73. Kern, T., Hediger, S., Muller, P., Giustini, C., Joris, B., Bougault, C., Vollmer, W., and Simorre, J. P. (2008) Toward the characterization of peptidoglycan structure and protein—Peptidoglycan interactions by solid-state NMR Spectroscopy. *J. Am. Chem. Soc. 130*, 5618.
74. Meroueh, S. O., Bencze, K. Z., Hesek, D., Lee, M., Fisher, J. F., Stemmler, T. L., and Mobashery, S. (2006) Three-dimensional structure of the bacterial cell wall peptidoglycan. *Proc. Natl. Acad. Sci. U. S.A. 103*, 4404–4409.
75. Cegelski, L., Kim, S. J., Hing, A. W., Studelska, D. R., O'Connor, R. D., Mehta, A. K., and Schaefer, J. (2002) Rotational-echo double resonance characterization of the effects of vancomycin on cell wall synthesis in *Staphylococcus aureus*. *Biochemistry 41*, 13053–13058.
76. Kim, S. J., Cegelski, L., Preobrazhenskaya, M., and Schaefer, J. (2006) Structures of *Staphylococcus aureus* cell-wall complexes with vancomycin, eremomycin, and chloroeremomycin derivatives by C-13{F-19} and N-15{F-19} rotational-echo double resonance. *Biochemistry 45*, 5235–5250.
77. Cegelski, L., Steuber, D., Mehta, A. K., Kulp, D. W., Axelsen, P. H., and Schaefer, J. (2006) Conformational and quantitative characterization of oritavancin-peptodoglycan complexes in whole cells of *Staphylococcus aureus* by in vivo C-13 and N-15 labelling. *J. Mol. Biol. 357*, 1253–1262.
78. Mehta, A. K., Cegelski, L., O'Connor, R. D., and Schaefer, J. (2003) REDOR with a relative full-echo reference. *J. Magn. Reson. 163*, 182–187.
79. Kim, S. J., Cegelski, L., Studelska, D. R., O'Connor, R. D., Mehta, A. K., and Schaefer, J. (2002) Rotational-echo double resonance characterization of vancomycin binding sites in *Staphylococcus aureus*. *Biochemistry 41*, 6967–6977.
80. Tong, G., Pan, Y., Dong, H., Pryor, R., Wilson, G. E., and Schaefer, J. (1997) Structure and dynamics of pentaglycyl bridges in the cell walls of *Staphylococcus aureus* by C-13-N-15 REDOR NMR. *Biochemistry 36*, 9859–9866.
81. Shenouda, N. S., Pan, Y., Schaefer, J., and Wilson, G. E. (1996) A simple solid-state NMR method for determining peptidoglycan crosslinking in *Bacillus subtilis*. *Biochm. Biophys. Acta 1289*, 217–220.
82. Pan, Y., Shenouda, N. S., Wilson, G. E., and Schaefer, J. (1993) Cross-links in cell-walls of *Bacillus subtilis* by rotational-echo double-resonance N-15 NMR. *J. Biol. Chem. 268*, 18692–18695.
83. Forrest, T. M., Wilson, G. E., Pan, Y., and Schaefer, J. (1991) Characterization of cross-linking of cell-walls of *Bacillus subtilis* by a combination of magic-angle spinning NMR and gas-chromatography mass-spectrometry of both intact and hydrolyzed C-13-labeled and N-15-labeled cell-wall peptidoglycan. *J. Biol. Chem. 266*, 24485–24491.
84. Schaefer, J., Garbow, J. R., Jacob, G. S., Forrest, T. M., and Wilson, G. E. (1986) Characterization of peptidoglycan stem lengths by solid-state C-13 and N-15 NMR. *Biochem. Biophys. Res. Commun. 137*, 736–741.
85. Jacob, G. S., Schaefer, J., and Wilson, G. E. (1983) Direct measurement of peptidoglycan cross-linking in bacteria by N-15 nuclear magnetic-resonance. *J. Biol. Chem. 258*, 824–826.
86. Jacob, G. S., Schaefer, J., and Wilson, G. E. (1983) Direct measurement of peptidoglycan cross-linking in *Aerococcus viridans* using solid-state N-15 nuclear magnetic-resonance. *Fed. Proc. 42*, 2127–2127.
87. Kim, S. J., Matsuoka, S., Patti, G. J., and Schaefer, J. (2008) Vancomycin derivative with damaged D-Ala-D-Ala binding cleft binds to cross-linked peptidoglycan in the cell wall of *Staphylococcus aureus*. *Biochemistry 47*, 3822–3831.
88. Patti, G. J., Chen, J. W., Schaefer, J., and Gross, M. L. (2008) Characterization of structural variations in the peptidoglycan of vancomycin-susceptible *Enterococcus faecium*: Understanding glycopeptide-antibiotic binding sites using mass spectrometry. *J. Am. Soc. Mass Spectrom. 19*, 1467–1475.
89. Patti, G. J., Kim, S. J., and Schaefer, J. (2008) Characterization of the peptidoglycan of vancomycin-susceptible *Enterococcus faecium*. *Biochemistry 47*, 8378–8385.
90. Kumar, S., and Nussinov, R. (1999) Salt bridge stability in monomeric proteins. *J. Mol. Biol. 293*, 1241–1255.
91. Kumar, S., and Nussinov, R. (2002) Relationship between ion pair geometries and electrostatic strengths in proteins. *Biophys. J. 83*, 1595–1612.